JOURNAL OF MATERIALS SCIENCE 30 (1995) 4492–4506

Morphology of surface crystallites on amorphous $Fe_{87}Zr_7B_5Cu_1$

J. D. AYERS, J. H. KONNERT, P. DANTONIO, A. PATTNAIK, C. L. VOLD, H. N. JONES
Naval Research Laboratory, Washington, DC 20375-5320, USA

Surface crystallites a few tens of nanometres in breadth have been observed on the as-melt-spun surface of an alloy of composition $Fe_{87}Zr_7B_6Cu_1$. These crystallites are preferentially oriented, and exhibit a (2 0 0) texture. Heat treatments at temperatures in the interval 623–773 °C caused the surface grains to coarsen and new, randomly oriented crystals to form. Compositional inhomogeneities were found to contribute to the formation of the surface crystallites. Results suggest that surface energy effects are more important during the nucleation of crystallites in the liquid than they are below the glass transition temperature.

1. Introduction

The alloy studied here, which can be made amorphous by rapid quenching from the molten state, exhibits attractive soft magnetic properties when crystallized [1, 2]. When properly heat-treated (i.e. at 873 K for 3.6 ks), this alloy exhibits a microstructure consisting of body centred cubic (b.c.c.) structure crystallites only about 10 nm in diameter [1, 2]. There appears to be no mention in the literature of surface crystallites in this alloy, but surface crystallites have been observed to form more readily than those within the bulk of various amorphous alloys [3], including Fe–Zr alloys with 8–10% Zr [4] and $Fe_{87}B_{13}$ [5]. Surface crystallites can grow as a primary phase (i.e. with the crystal structure of the major constituent), or they can grow eutectically or polymorphically (i.e. as a single phase intermetallic compound having the same composition as the glass). Surface crystallites formed on amorphous Fe-based alloys often have the b.c.c. structure of ferritic Fe, though face centred cubic (f.c.c.) crystallites are formed on $Fe_{70}Ni_{10}B_{20}$ [3] and $Fe_{87}B_{13}$ [5]. Surface crystals of more complex structure form in many alloys, particularly when they grow to depths greater than a few hundred nanometres. Amorphous Fe-based alloys with b.c.c. crystalline surfaces have been found to exhibit (2 0 0) or (2 2 2) growth textures [4, 6], while (1 1 1) and (2 2 0) textures have been reported on those with f.c.c. surface crystallites [5, 6].

Surface crystallites can be formed either during the initial quench from the melt or during subsequent heat treatment. Matsuura [4] found that b.c.c. crystals formed at the free surface of Fe–Zr alloys during melt spinning only when the Zr content was below 10%, and that it became progressively more difficult to suppress surface crystallization as the Zr content was lowered. Matsuura also found that the surface crystallites could be removed by polishing about 1 μm from the free surface, and he found that in a $Fe_{91}Zr_9$ alloy they grew to a depth of approximately 3 μm during a 900 s heat treatment at 825 K. Surface crystallites formed during rapid solidification in air or during reheating in oxygen-containing atmospheres are often associated with surface oxidation or the loss of one of the alloying elements from the surface [3]. Fujinami and Ujihira [7] studied the surface and bulk crystallization of an $Fe_{90}Zr_{10}$ alloy in air and in vacuum using transmission Mössbauer spectroscopy, conversion electron Mössbauer spectroscopy, and Auger electron spectroscopy (AES). They found that surface crystals formed at temperatures as low as 473 K on samples heat treated in both air and vacuum, whereas crystallization in the centre portion of their thin ribbons occured only at temperatures some 340 K higher in the vacuum (0.13 Pa) heat-treated samples and about 300 K higher in the air processed samples. The AES studies showed a thin (10–30 nm thick) oxygen-rich surface layer even on the as-melt-spun samples and a deeper oxygen-enriched layer on heat-treated samples. They conclude that because the conversion electron Mössbauer spectroscopy (which probes the atomic environment of the Fe in about the outer 300 nm of the sample) showed no evidence of iron oxide, oxygen had removed the Zr from solution and promoted formation of the surface crystallites.

Relatively little study has been made of the morphology of primary phase surface-nucleated crystallites, in part because they are often too small to resolve with optical or scanning electron microscopy (SEM). A study of metallic glasses by Watanabe and Nakamura [8] using atomic force microscopy (AFM) reported that as-melt-spun $Fe_{78}B_{13}Si_9$ was covered with holes a few nm wide and about 1 nm deep, some of which had a small bump at their bottom. After low temperature heat treatment, some of the holes had multiple bumps in them, and, after treatments at higher temperatures, the holes were no longer evident

0022–2461

and the sample was covered with small protrusions with about the same spacing as the holes. It was concluded that the protrusions were crystallites nucleated at the bumps found in the initial holes.

In at least one instance [3] surface crystallites have been studied by transmission electron microscopy (TEM) of samples thinned from the reverse side, a tedious process. Other studies of surface crystallites have often been limited to techniques such as X-ray diffraction, Mössbauer spectroscopy, and compositional profiling by Auger analysis, which give results averaged over large surface areas. In this study, crystallographic parameters of the crystallites were characterized by X-ray techniques and surface chemistry was studied with scanning Auger microprobe analysis (SAM), while the morphology of surface crystallites was examined by SEM and AFM. The crystallites were examined in both the as-melt-spun condition and after heat treatments which coarsened them.

2. Experimental procedure

A button of the alloy $Fe_{87}Zr_7B_5Cu_1$, made from metals of 99.99% purity or better, was prepared by arc melting on a chilled Cu hearth in an argon atmosphere. Rapidly solidified ribbon was prepared by inductively melting the button in fused silica under He and ejecting the melt through a 0.5-mm diameter orifice onto the perimeter of a Cu wheel rotating at a surface speed of 48 m s^{-1}. The silica reacted to some extent with the alloy, with the result that the orifice was eroded to larger sizes during the course of melt spinning. For this reason, the width of the rapidly solidified ribbon increased from about 1 mm up to 3 mm and the thickness increased from about 12 μm up to about 25 μm.

Ribbon segments of diverse cross-section were examined by X-ray diffractometry to determine whether an amorphous structure had been achieved. Ribbon segments from all portions of the melt were found to exhibit some crystallinity on the free surface of the ribbon (i.e. the surface which did not contact the wheel during melt spinning). In addition to standard X-ray diffractometry, some samples were subjected to pole figure and rocking curve X-ray analyses in order to characterize the dispersion in orientations of the crystallites. All X-ray analyses were done on samples consisting of a parallel array of slightly overlapping ribbons affixed to a glass substrate with double-sided sticky tape. Results obtained are thus averaged over several ribbon segments.

Samples were prepared for heat treatment by encapsulating approximately 20 segments of ribbon, each approximately 30 mm long, in a 4-mm inside diameter borosilicate glass tubing which was first evacuated to a pressure of 4 Pa, flushed with He, pumped to the same pressure, and backfilled with He to a pressure of 5×10^4 Pa. The sealed capsules were 60 mm long, thus enclosing a volume of approximately 750 mm^3. Encapsulated samples were heat treated for 3.6 ks at temperatures ranging from 423 K up to 773 K in 50 K increments. All ribbon segments selected for encapsulation were approximately 15 μm thick and 1.5 mm wide.

The SAM analysis was carried out on the free surface of ribbon samples using a Perkin-Elmer Model 660 scanning Auger multiprobe. Analyses were done on probe areas about 100 μm^2 centred on 10-mm long, free-standing strips of ribbon in various conditions. The base vacuum was 6.65×10^{-8} Pa. Auger spectra were collected at 3 kV accelerating voltage with a specimen current of about 200 nA, while depth profiling was done with an ion gun operated at 3 kV. The sputtering rate was adjusted to about 4 nm min^{-1} (as calibrated with a stainless steel specimen). The peak height ratios of the elemental Auger peaks of interest were converted to atomic percentages using the elemental sensitivity factors obtained from the *Handbook of Auger Spectroscopy* [9].

3. Results

In order to simplify the presentation, experimental results are given in three subsections. The first and third, X-ray analysis and Auger analysis, give results averaged over the surface examined, while the microscopy section shows morphological observations.

3.1. X-ray analysis

The free surface of as-melt-spun ribbons exhibited X-ray diffraction patterns like that shown in Fig. 1. This pattern shows the broad maxima typical of amorphous metals and one sharp peak near 65 degrees 2Θ. This is the (2 0 0) peak of b.c.c. Fe, and in polycrystalline Fe it is normally only about 20% of the intensity of the (1 1 0) peak, which would be expected to show near to 45 degrees 2Θ. The absence of peaks other than (2 0 0) indicates that the crystallites have a preferred orientation, with (2 0 0) type planes nearly parallel to the sample surface. As mentioned in the introduction, this (2 0 0) texture has been seen for surface-nucleated crystallites in other Fe-based

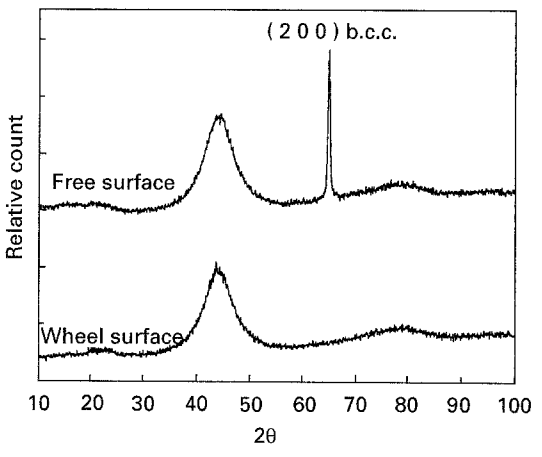

Figure 1 X-ray diffractometry trace from as-melt-spun sample showing two broad peaks from predominant amorphous phase and single narrow peak from surface nucleated b.c.c. phase.

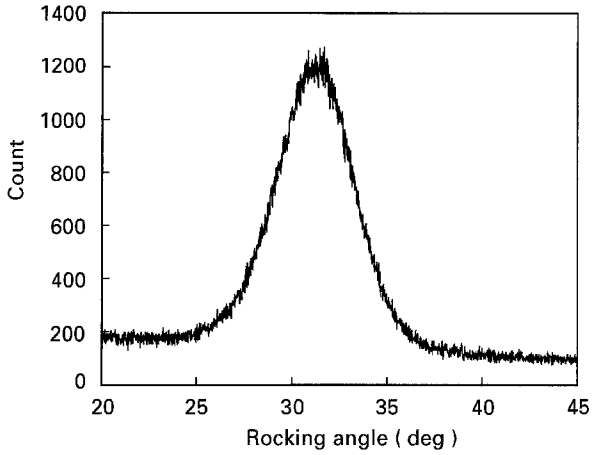

Figure 2 "Rocking curve" from (2 0 0) b.c.c. in Fig. 1, obtained by setting the Θ angle of the diffractometer at 5° and varying the detector angle, 2Θ, through the range of angles indicated.

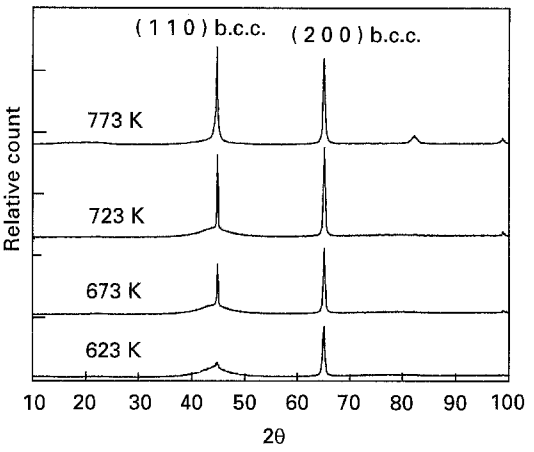

Figure 3 X-ray diffractometry traces from samples with surface crystallites like those of Fig. 1 after the samples were heat-treated for 3.6 ks at the temperatures indicated.

amorphous alloys. X-ray diffraction experiments on the surface of the ribbons which made contact with the chill wheel during melt spinning exhibited no sign of crystallinity.

Fig. 1 indicates that the surface crystallites have a (2 0 0) texture, but gives no indication of how much spread there is in their orientations. This was assessed by means of a rocking curve analysis, which consists of setting the detector of the diffractometer at the Bragg angle (65.01° with Cu$K_{\alpha 1}$ radiation) of the (2 0 0) plane and "rocking" the surface normal through the range of angles which will cause (2 0 0) planes near the surface normal to diffract. A 0.5° divergence slit was employed for the experiment. Results of this analysis are shown in Fig. 2. The rocking curve shown has a width at half the maximum which is just under five degrees, indicating that approximately 75% of the crystallites have ⟨1 0 0⟩ directions oriented within 2.5° of the surface normal. Some of the AFM images suggest that the surface crystallites may also have preferred directions in the plane of the surface. This possibility seemed unlikely, but it was tested by means of a (1 1 0) pole figure analysis of a sample which had been heated to 623 K for 3.6 ks. This analysis confirmed that the sample had a strong (2 0 0) texture, but gave no evidence that there were preferred directions in the plane of the free surface.

An initial objective of this study was to determine if the preferentially oriented surface dendrites could be made to grow into the interior of the ribbons. The primary test for success in this endeavour was X-ray diffraction of the heat-treated specimens. If the experiments had been successful, then the (2 0 0) peak would have grown at the expense of the broad intensity maxima from the amorphous phase. Fig. 3 demonstrates that this was not the case, for the (1 1 0) peak grew more than the (2 0 0) peak. The bottom curve in Fig. 3 is from the sample given the lowest temperature heat treatment which gave any detectable change in the diffraction pattern. The (2 0 0) peak is imperceptibly different from that of the as-spun sample shown in Fig. 1, but the (1 1 0) peak has begun to show. The curves for samples treated at higher temperatures show progressive strengthening of the (1 1 0) peak relative to that for (2 0 0) oriented crystallites. This indicates that randomly oriented crystals exhibit more growth than the preferentially oriented surface crystallites. The X-ray measurements do not show whether the new crystals formed on the free surfaces or in the interior of the ribbons, but the microscopy studies showed that many of them were at the free surface.

3.2 Microscopy

The two microscopic techniques employed (SEM and AFM) yielded substantially different types of information about the samples examined. As is widely appreciated, SEM provides invaluable results when large areas are to be examined or when large depths of field are required, whereas AFM is better suited for examining smaller areas at high resolution. SEM examination of the as-melt-spun ribbons showed their macroscopic morphology, but gave no evidence of crystallinity on the sample surfaces. Macroscopic features could be imaged only with difficulty in AFM, but it showed a wealth of small scale morphological detail. This detail was found to vary from region to region on a sample and from sample to sample on different segments taken from the same ribbon.

Some areas of the as-melt-spun sample were found to be free of crystals of any size and showed the characteristics of an amorphous metal, evident in Fig. 4. In this figure and the other AFM images shown here, the colour scale to the right shows the range of height variations in the area probed. From the scale presented in Fig. 4, one can see that over small distances, undulations of the surface are less than 1 nm high. A measurement of the average roughness of this surface showed a standard deviation of only 0.2 nm from a plane fit to the area. In contrast to this nearly perfect surface, some areas of as-melt-spun samples were covered by crystallites of varying morphologies. In some samples, large areas of the surface were covered with tiny crystallites of the type evident in Fig. 5. These crystallites vary in size from approximately 20 nm up to about 65 nm. They are not

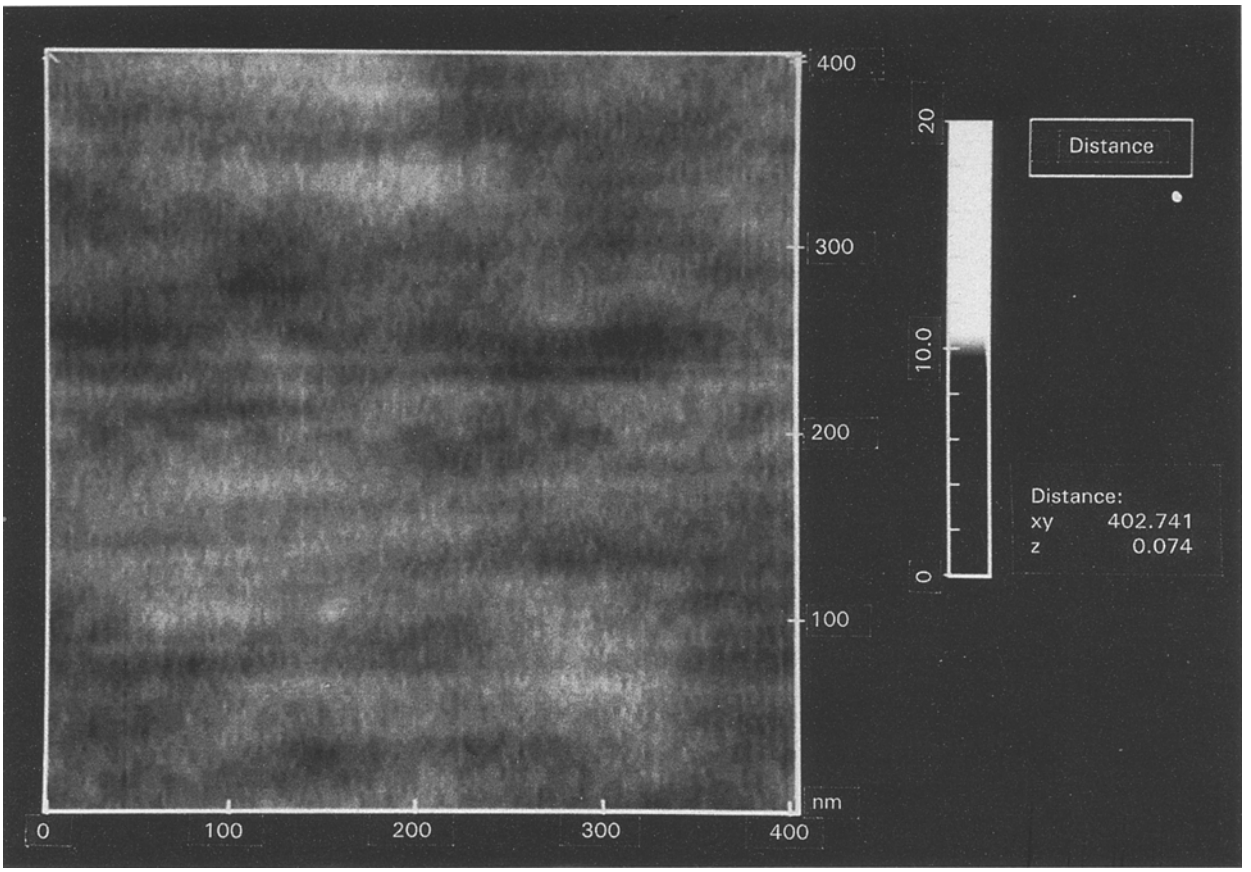

Figure 4 Atomic force microscopy image from surface area quenched rapidly enough to prevent the formation of any detectable crystallization.

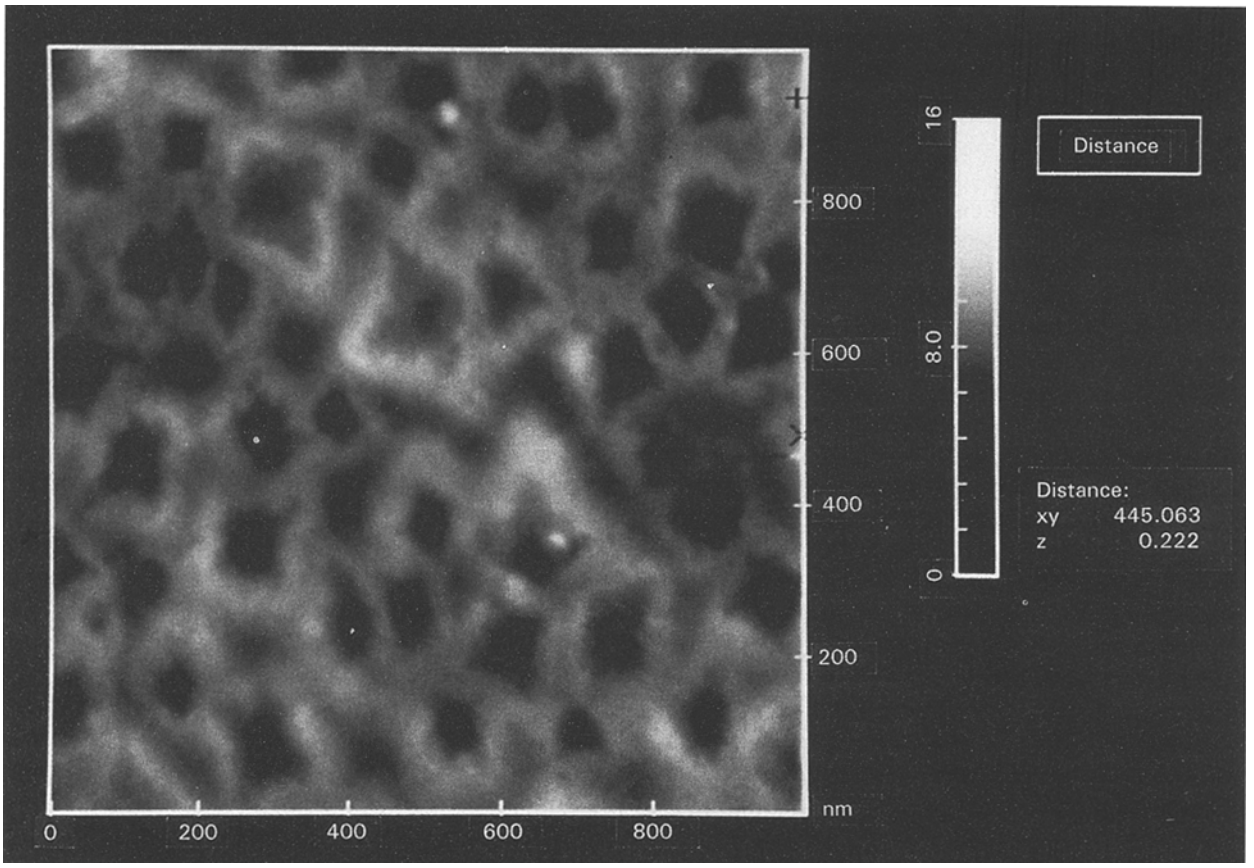

Figure 5 Small features on surface of sample quenched at a rate inadequate to suppress surface crystallization.

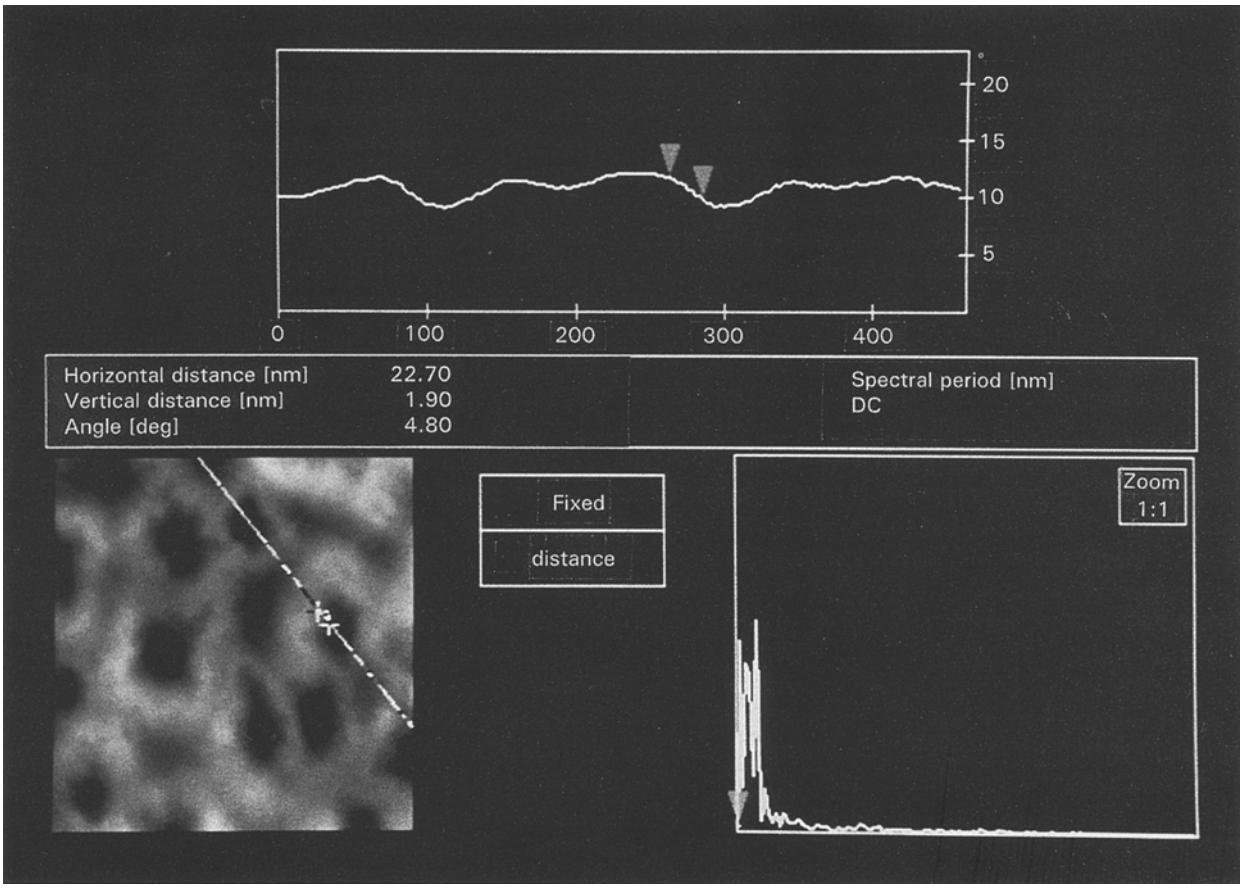

Figure 6 A portion of the image in Fig. 5 is shown in the lower left, while the upper line drawing shows a height profile along a trace indicated by the line in the lower left figure. The spectrum analysis at the lower right is uninteresting because the trace has no short period height undulations.

sufficiently well resolved in the figure to positively identify crystallographic features, but many of them are nearly rhombic in shape. Because the X-ray measurements show that most of the crystals have (200) type crystallite planes nearly parallel to the sample surface, it is reasonable to conclude that the rhombuses are crystallites and that their apexes point in ⟨100⟩ directions which are normal to the free surface. Surprisingly, the centres of all crystallites of this type are lower than the surrounding glass, the depression being as great as about 4 nm. A striking feature of these crystallites is that many are surrounded by a ridge of glassy metal which is elevated above the surrounding glass. In some samples there were regions with small crystallites which did not show the ridges evident in Fig. 5.

As part of an effort to better understand the shape of the free surface in the vicinity of the small crystallites which do show the elevated ridges, surface profiling was done along lines running across some of the precipitates. The results of one of these experiments are shown in Fig. 6. Fig. 6(a) shows an enlarged section from Fig. 5 and includes the trace from which the profile in Fig. 6(b) was measured. The profile clearly demonstrates the depression in the centre of one of the precipitates and the hump in the adjacent glass. The two triangular markers in Fig. 6(b) were placed to permit measurement of surface tilting between them. The positions of these markers in Fig. 6(a) are indicated by crosses. The angle that the trace between the two markers makes with the surface plane was found to be 4.8°. Similar measurements on other precipitates gave maximum inclinations ranging from about 4° to 6°. The presence of this ridge surrounding the crystallites suggests that they formed when the melt was above the glass transition temperature, and that the surface was bowed by surface tension effects at the melt/crystal/vapour junction. This effect will be considered in Section 4.

In the widest portion of the melt spun ribbon, in which the thickness was as great as 25 μm, the surface crystallites were somewhat more developed than those shown in Fig. 5. In some areas the surface appears to be fully converted into crystallites similar in size and shape to those in Fig. 5, while in other areas the crystallites exhibit the rounded morphology evident in Fig. 7. It is not clear how these knobs relate to the structure of the underlying crystallites.

When the samples were heat treated, new crystallites were formed and substantial coarsening of the structures occurred. Because the structure of the starting material varied from area to area, quantitative study of the coarsening was not practical, but the qualitative results are interesting. At the higher temperatures employed for heat treatments, the microstructural evolution was quite pronounced. The four images in Fig. 8 are representative of structures seen on the samples whose X-ray diffraction traces are given in Fig. 3. While the appearance of the structures in the samples illustrated in Fig. 8 do not vary

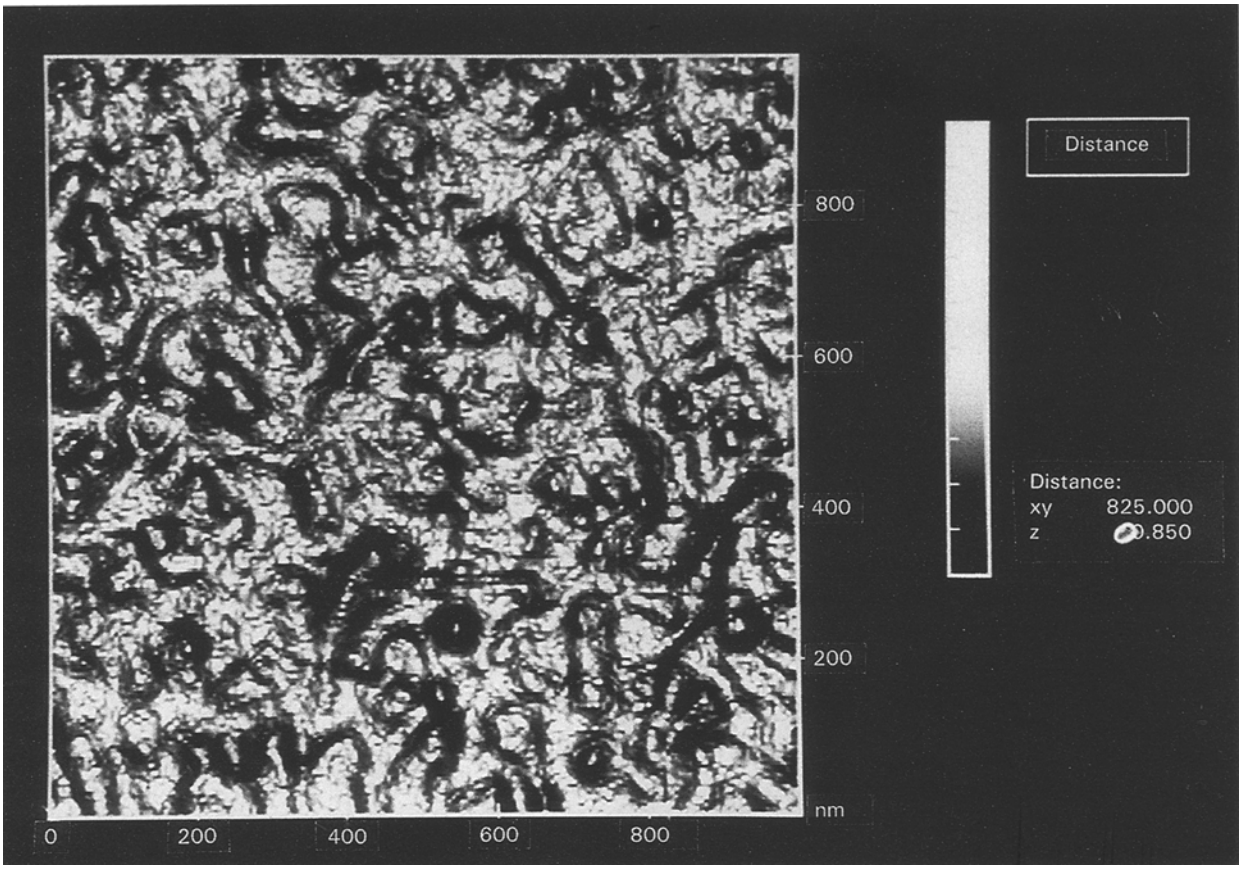

Figure 7 Atomic force microscopy images showing surface morphology on a thick portion of the ribbon. X-ray diffractometry shows that the major portion of material in ribbons with such surfaces were amorphous.

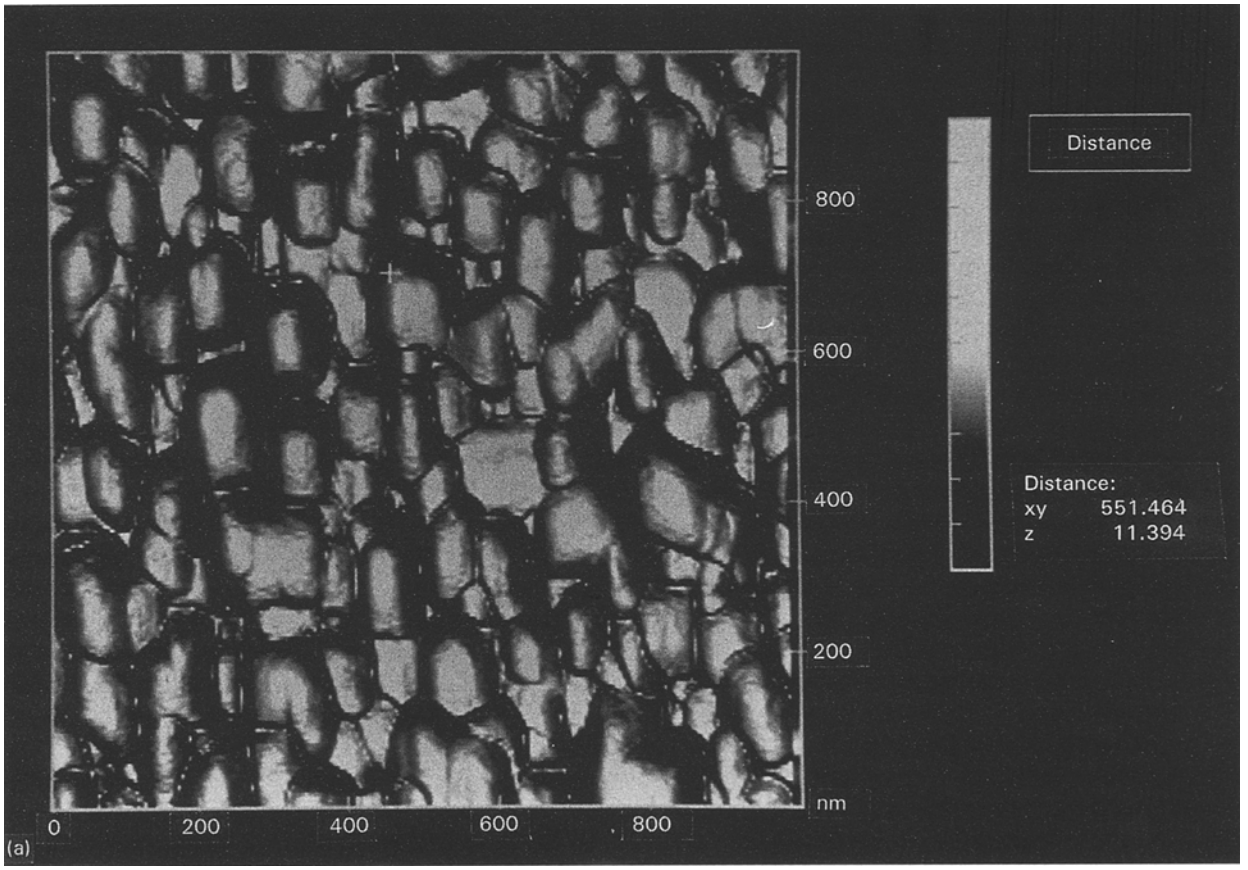

Figure 8 Atomic force microscopy images of surface crystallites on the samples whose diffractometry traces are shown in Fig. 3. Parts (a) to (d) were heat-treated at progressively higher temperatures. The RMS surface roughnesses are as follows: (a) 10.5 nm; (b) 13.5 nm; (c) 15.0 nm; (d) 31.5 nm.

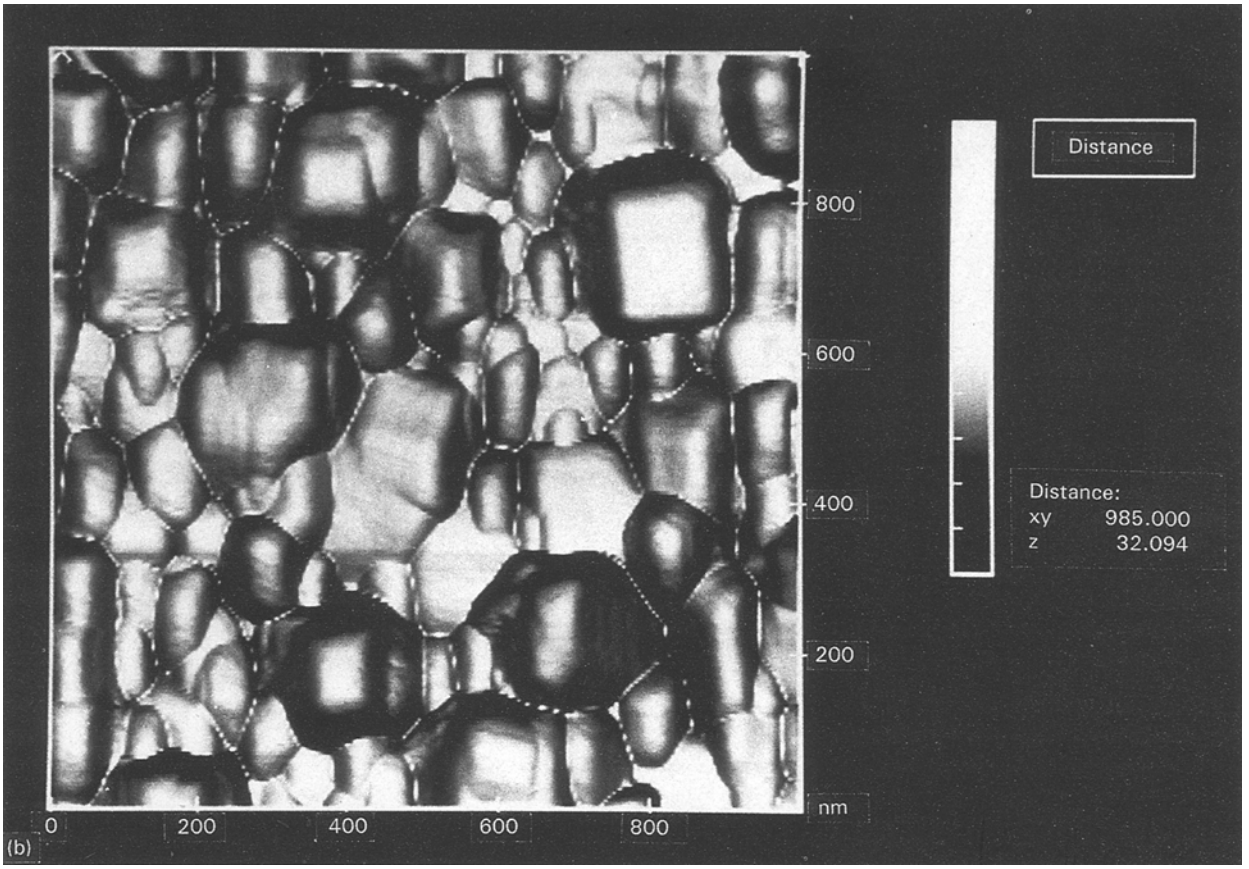

Figure 8b Continued

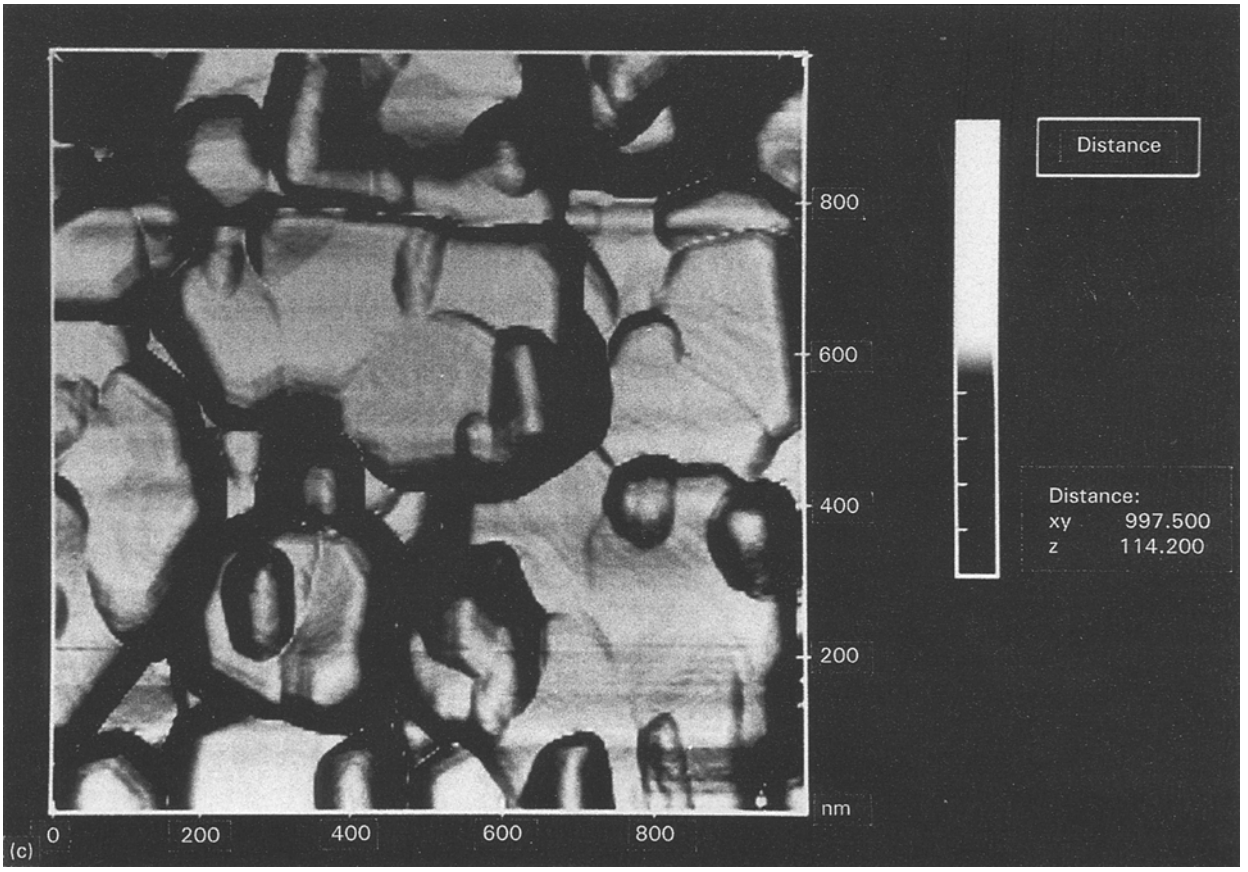

Figure 8c Continued

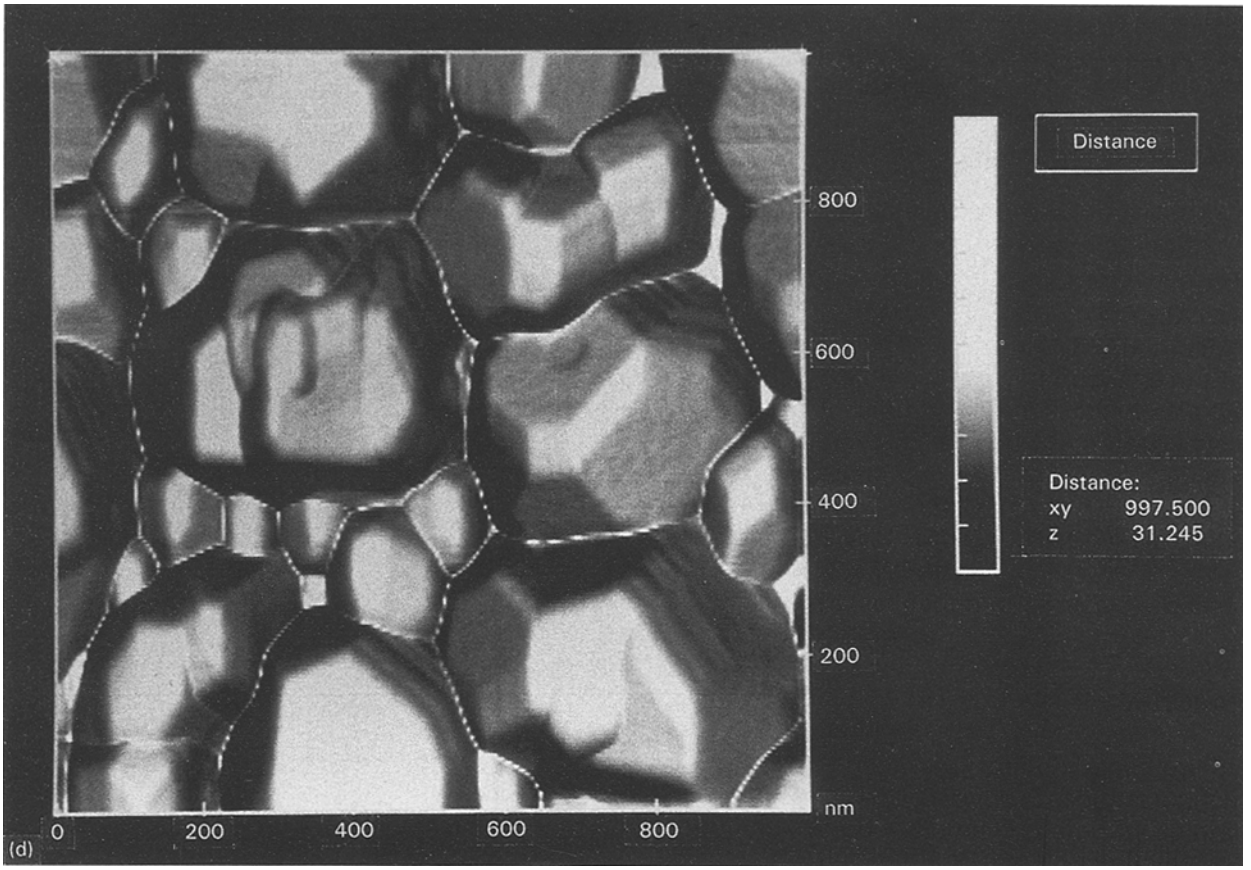

Figure 8d Continued

substantially across their surfaces, the size of the crystallites do change somewhat from area to area. This variation within a sample is smaller than the differences between samples heated to different temperatures. The photographs in Fig. 8 demonstrate a dramatic growth in the crystal size with increasing temperature, and also a large increase in roughness, particularly at the highest heat-treating temperature. It is unlikely that the coarsening exhibited in Fig. 8 could have occurred if the surface crystallites were separated by an amorphous film such as that which prevents grain growth in the interior portions of the alloy studied here [2]. The surface crystals can therefore reasonably be called grains, and the boundaries separating them grain boundaries. It is interesting that these surface grains should develop such pronounced faceting during heat treatment. Many of the planar features obviously coincide with the low index planes of b.c.c. Fe.

While the microstructures shown in Fig. 8 can be discussed strictly in terms of grain growth, samples heated to lower temperatures exhibit more varied structures. A sample heated to 523 K for 3.6 ks had some areas which still appeared to be amorphous and some which were similar to Fig. 5. These are shown in Fig. 9(a). These small structures are recessed into the surface, like those in the unheated sample, and many of them have arms, which must correspond to $\langle 1\,0\,0 \rangle$ growth directions; the surrounding glass does not exhibit the curvature evident in the more developed crystallites shown in Figs 5 and 6. These crystallites are very similar to some seen in as-melt-spun samples, suggesting that they were present before the heat treatment. Some of the features of this type did, however, have small bumps near them, as illustrated in Fig. 9(b). These bumps are similar in appearance to the knobs seen in Fig. 7(b), though they are somewhat less developed. There is no clear relationship between the bumps and the recessed crystallites. The sample heated to the next higher temperature, 573 K, had some areas which were similar in appearance to Fig. 9, as well as areas like that in Fig. 10. The bumps shown in Fig. 10 are similar to that in Fig. 9(b), but they are more numerous than was the case at the lower temperature, and they are larger. The mounds in Fig. 10 appear not to be associated with the depressed crystallites shown in Figs 5 and 9, so they probably nucleated independently of such features. It appears, however, that the smaller mounds may have nucleated in association with the larger ones. It is perhaps also noteworthy that the mounds exhibit no evidence of the faceting seen on the larger crystallites produced at higher temperatures.

Whereas little was learned by SEM investigation of the as-melt-spun surfaces, the technique provided much insight when applied to the heat-treated samples, particularly those treated at the higher temperatures. Fig. 11 demonstrates that variations in surface structure could be discerned in the 773 K heat-treated sample, even at relatively low magnifications. This photograph shows that some areas of the surface are substantially brighter in the secondary electron detection mode than are others. Fig. 12, taken at a higher magnification, demonstrates that in some areas

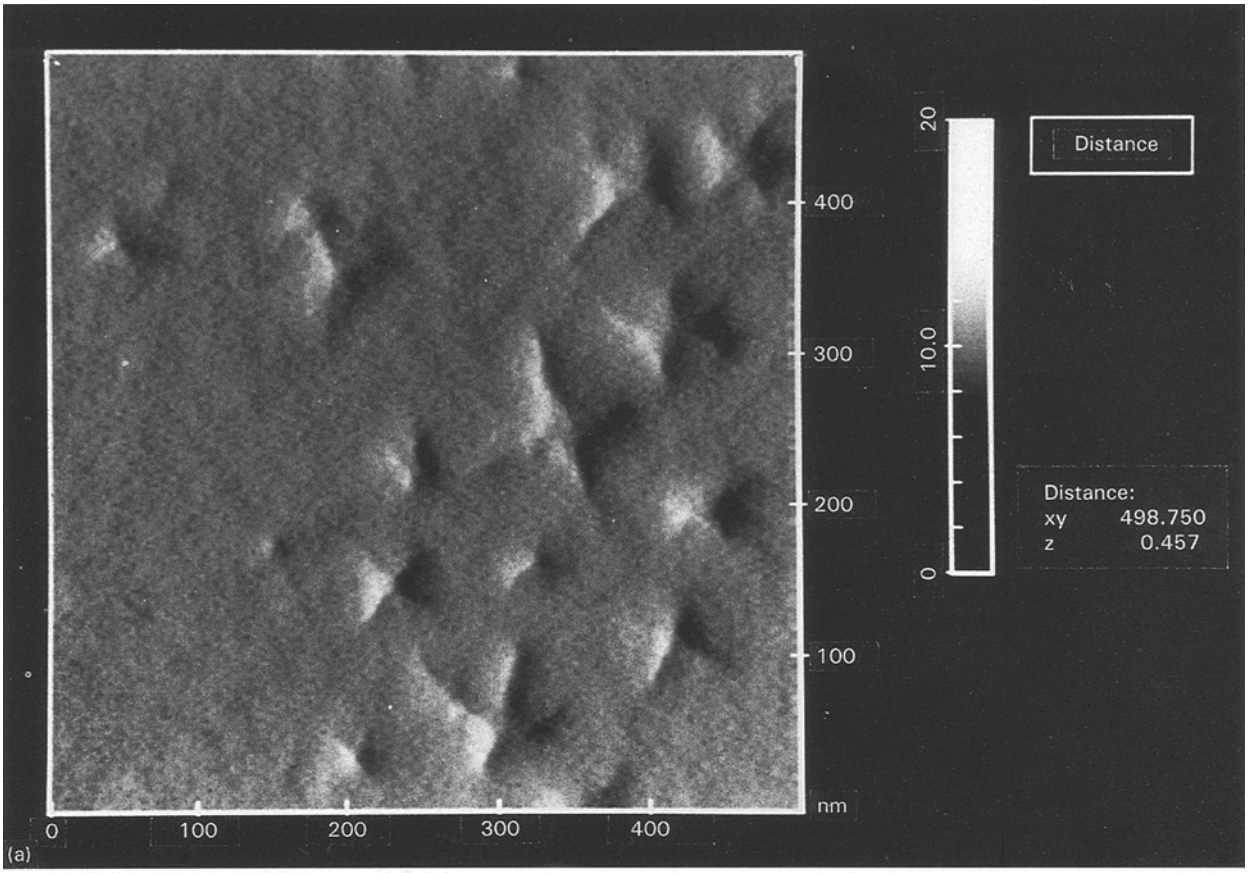

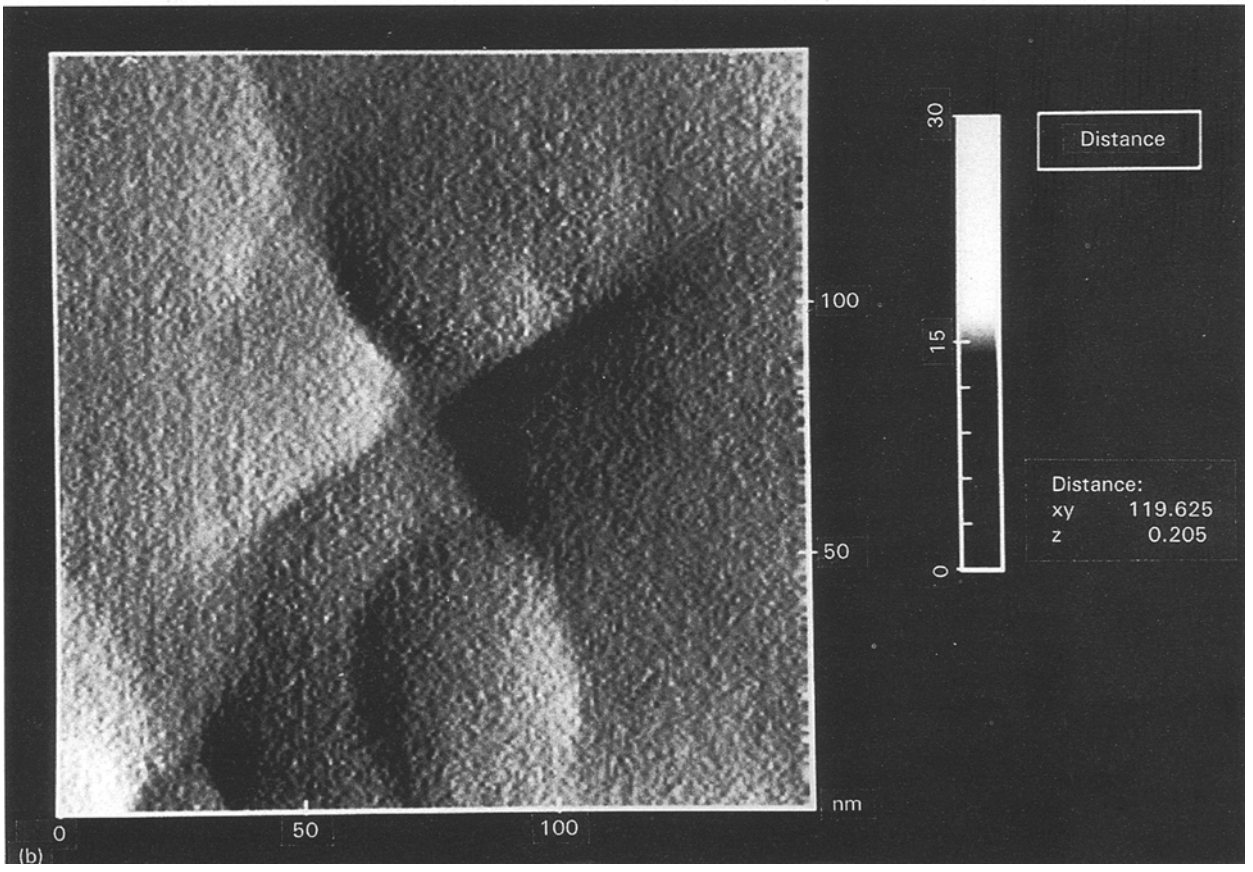

Figure 9 Small features on surface of a sample heat-treated for 3.6 ks at 573 K. Some areas had only the concave features shown in (a), while others had a few small bumps like that shown in (b).

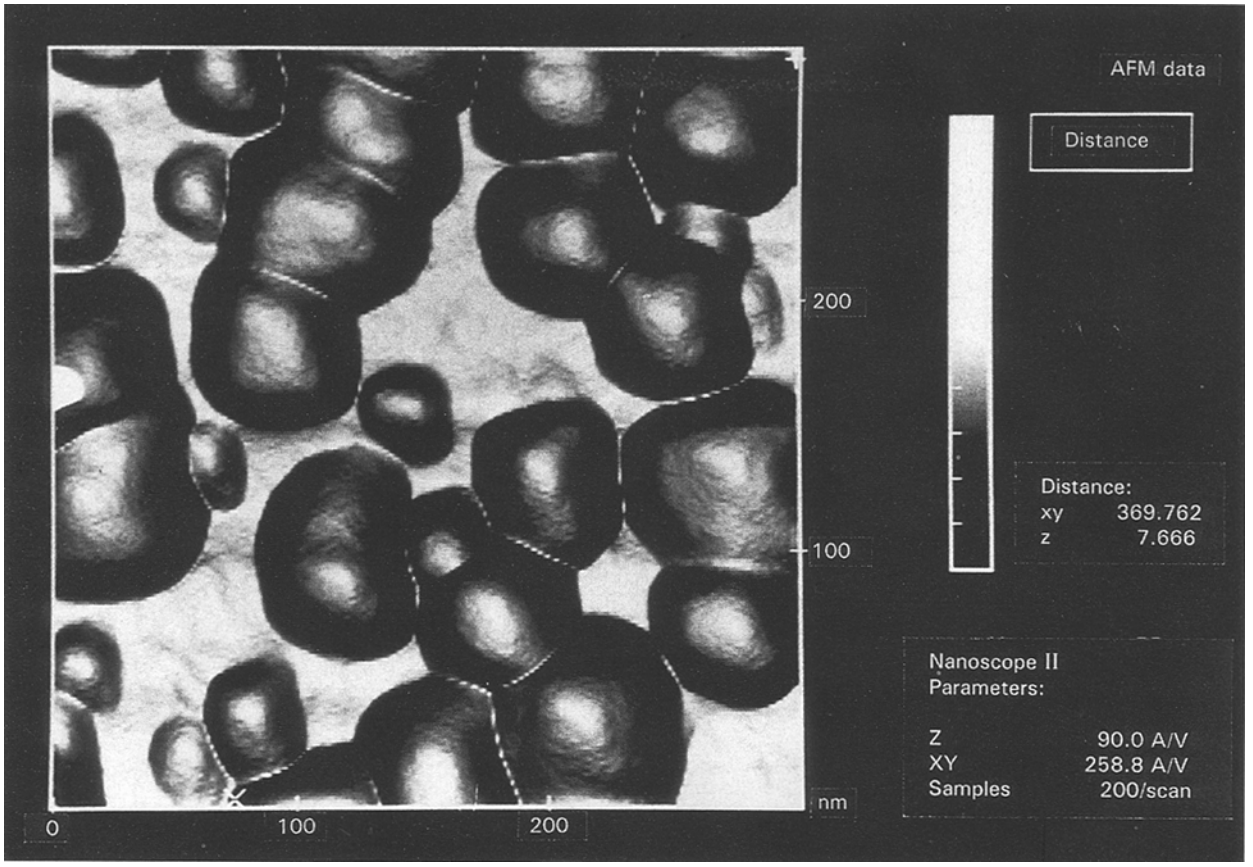

Figure 10 Small, convex features on surface of a sample heat-treated for 3.6 ks at 573 K.

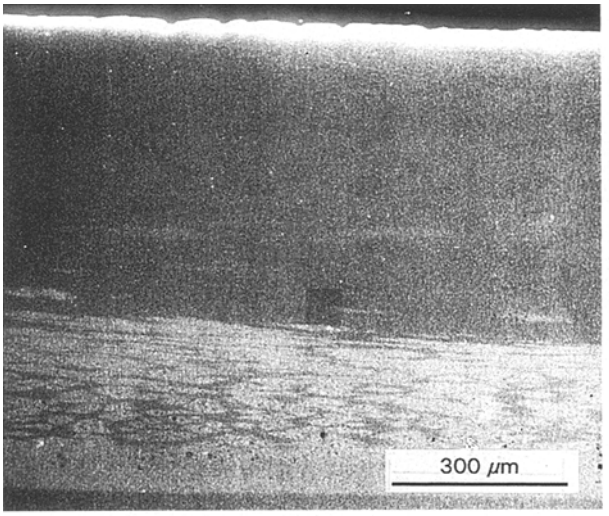

Figure 11 Scanning electron microscopy image of sample heat-treated for 3.6 ks at 773 K.

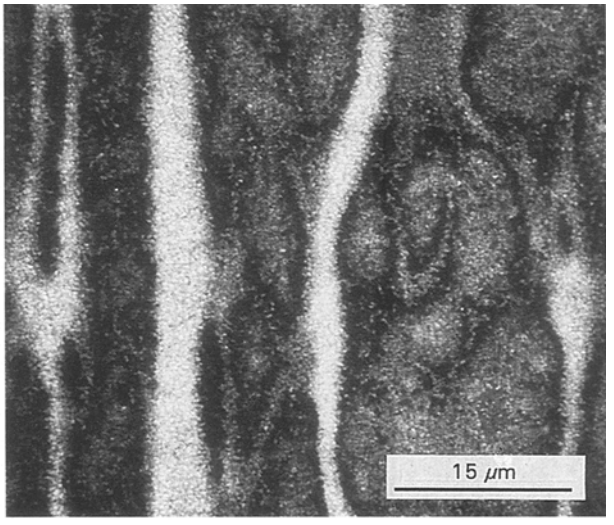

Figure 12 View at an intermediate magnification of a portion of the sample pictured in Fig. 11.

the brighter and darker areas interpenetrate on a micrometre distance scale, and it further shows that the bright contrast stripes have features reminiscent of convective flow lines in liquids. Study of the same surface at yet higher magnification showed that both the darker areas and the lighter areas are covered with resolvable crystals, and that the darker appearing regions have finer surface grains than do the brighter areas. This difference is demonstrated in Fig. 13, wherein it can be seen that the grain size in the bright area is at least twice that in the darker area. A rationale for the observed differences in electron emissivity and grain size was provided by studying the two regions in SEM with energy dispersive spectroscopy (EDS). The energy spectra obtained are shown in Fig. 14. Note that the curves show no peaks for boron (because of its low atomic number) or copper (because it constituted only 1 at % of the alloy). In order to permit semiquantitative comparison of the two regions, energy windows were set at the Zr *L* peak (1675–2275 ev) and the Fe *K* peak (6125–6625 ev). Counting was not done at

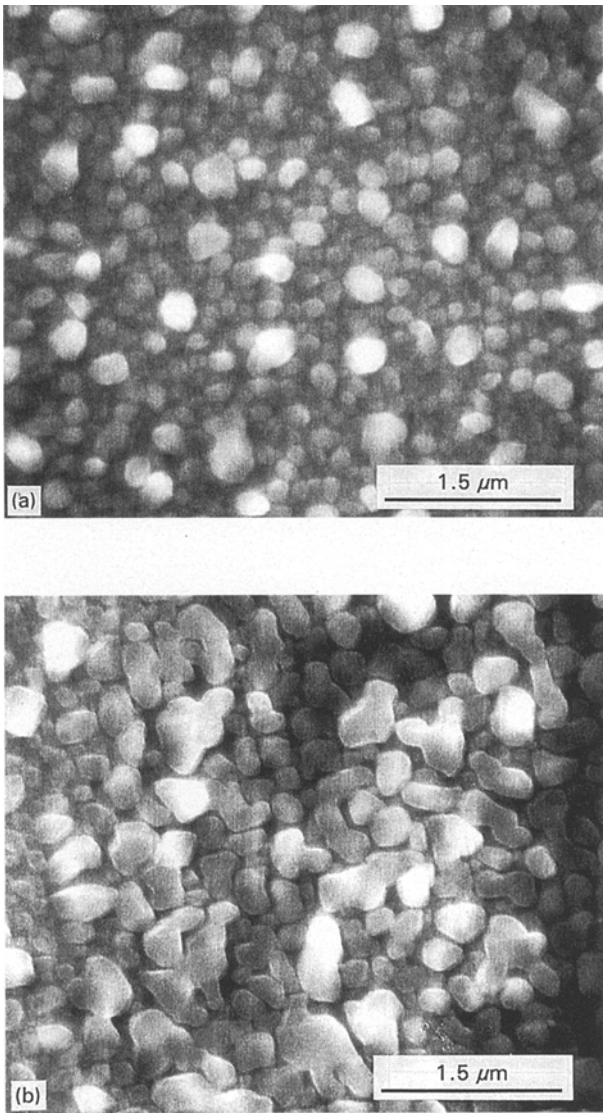

Figure 13 High magnification views of areas from Fig. 11 which have darker contrast, in (a), and brighter contrast, in (b).

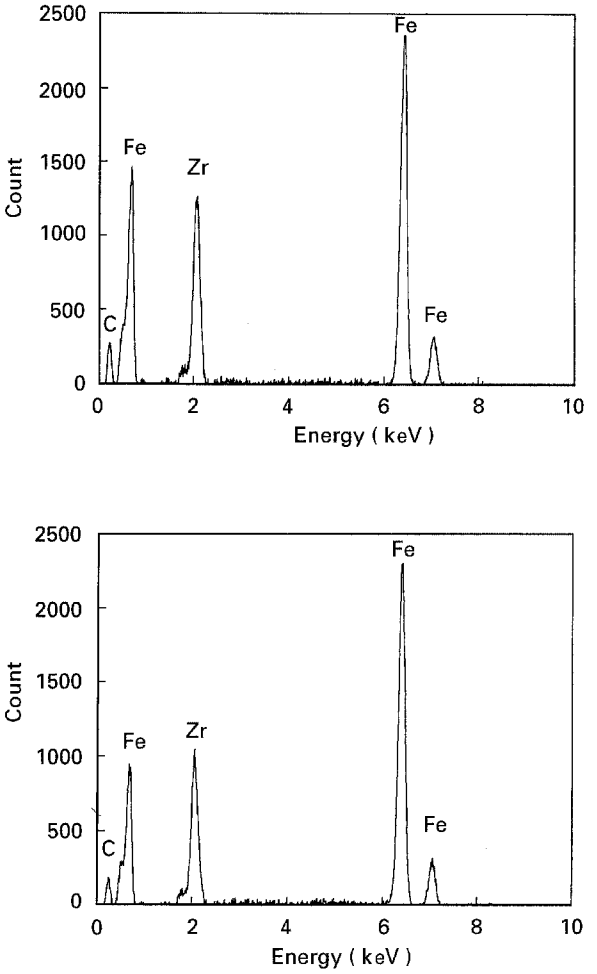

Figure 14 Energy dispersive analysis spectra from areas of darker and brighter contrast in Fig. 11. Parts (a) and (b) are arranged as in Fig. 13.

the Fe L peak because this peak is partially overlapped by an oxygen peak. The number of counts obtained from each of the four peaks examined are shown next to their respective peaks in Fig. 14. The integrated intensity ratios, I_{Zr}/I_{Fe} for the two peaks were 0.58 in the darker area and 0.48 in the brighter area. These data show that the molten alloy was not compositionally homogeneous prior to melt spinning, for such partitioning would not be possible during the solidification time available. The differences in grain sizes obviously result from this compositional variation.

3.3. Scanning auger microprobe analysis

Auger analysis was undertaken in an effort to determine if surface oxidation might have effected the rates of surface crystallite formation and coarsening. It was motivated by the observation of others [3, 7] that oxidation can promote surface crystallization, and also by the observation that the as-melt-spun samples and those heat-treated at modest temperatures appear shiny and bright silver-grey to the eye, while those heat-treated at the highest temperatures appear dull and darker grey. The SAM results are summarized in Fig. 15, wherein (a), (b) and (c) show the results from an as-melt-spun sample, a sample heated to 623 K, and one heated to 773 K, respectively. The data shown in these graphs have been normalized to show the atomic percentages of the four elements studied. These measurements gave Fe concentrations inside the oxygen-rich surface layer which are somewhat higher than expected from as-weighed compositions, while the Zr and B concentrations are lower than expected. No calibration standards were employed, so the uncertainty in concentrations is at least $\pm$ 20%, and these differences may not be significant. Although the uncertainty in absolute concentrations is high, the relative uncertainty for the experiments is only about $\pm$ 10%.

Considering now the measured concentration variations with depth, and examining Fig. 15(a) first, it can be seen that the oxygen peak was quite high initially, but dropped to a lower, nearly constant value after about twenty minutes of sputtering, while the initially low Fe concentration increased to a high, nearly constant value in the same time. Calibration tests done with stainless steel specimens have shown that with the conditions employed here, the surface is eroded at a rate of about 0.4 nm min^{-1}, and the alloy studied here should sputter at about the same rate. It therefore

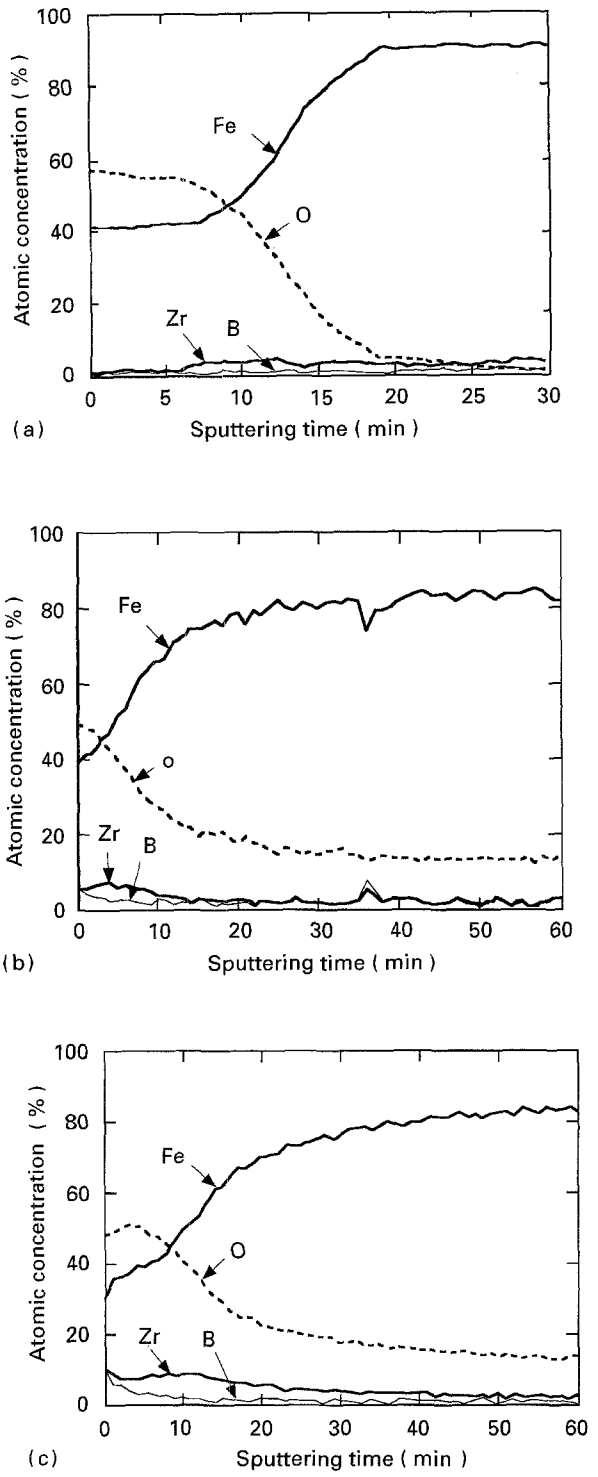

Figure 15 Scanning Auger microprobe analysis of as-melt-spun sample, (a), and of samples heat-treated at 623 and 773 K, respectively, in (b) and (c).

appears that during melt spinning, the surface was partially oxidized to a depth of about 8 nm. One might expect this oxidized surface layer to be enriched in Zr and B, since the oxides of these elements are more stable than those of Fe, but the data shown in Fig. 15(a) give no evidence that this is true. The Zr and B curves of this figure are, if anything, lower near the surface than they are at depth, but this apparent lowering probably results merely from dilution caused by the oxygen pickup (as does that for Fe). In Fig. 15(b) and (c), on the other hand, the Zr and B concentrations appear to be slightly higher near the surface than they are at greater depths. These increases may result from the diffusion of these elements to the surface from greater depths. This may well have been possible, for it is clear from Fig. 15(b) and (c) that during the heat treatments oxygen diffused to depths substantially greater than that sputtered away in 62 min (about 25 nm). In these samples the oxygen concentrations near the surfaces are similar to those in Fig. 15(a), and they drop substantially in the outer 8–10 nm, but thereafter they remain nearly constant. The concentration indicated in the nearly constant zone, 10–15 at %, is substantially higher than the amount of oxygen b.c.c. iron should dissolve. This point will be considered in the discussion.

4. Discussion

The variations in Zr concentrations found by SEM and EDS analysis obviously had a strong influence on the ease of formation of the surface crystallites during melt spinning, as well as influencing the rate at which they grow during heat treatment. The larger grain size in the lower Zr content area pictured in Fig. 13(b) makes it clear that Zr slows the kinetics of grain growth on the surface. These observations are consistent with the findings of Matsuura [4] that surface crystallites are progressively more difficult to suppress in binary alloys containing less than 10% Zr. Because the concentration measurements made here were not quantitative, it is not clear how strong the effect is. The low apparent Zr and B concentrations found by SAM suggest that a portion of these alloying additions may have been lost, either during the initial arc melting or, more likely, during inductive melting in fused silica for melt spinning. The observed concentration fluctuations may have resulted from incomplete melting in the fused silica, or they have resulted from the melt/crucible interaction noted above. The nature of the melt/crucible interaction has not been investigated, but it was probably not as simple as a reduction of the SiO_2 by the Zr and/or B in the melt, because no evidence of Si was found in either EDS or SAM. The SiO_2 crucible had a substantial, dark coloured skull remaining in it afterwards, so the interaction products were largely insoluble at the melt temperature. Given these diverse observations, it must be concluded that the morphological results may not be characteristic of the exact alloy composition specified in the title of this paper, but they are, nevertheless, interesting.

The oxygen-rich surface layer on the as-melt-spun ribbon is so thin (about 8 nm) that it would not be expected to provide a strong mechanical constraint on the nucleation and growth of crystallites, but it may well have an important chemical effect. As will soon be discussed, the interfacial free energies of the various phases present at the free surface during nucleation of the crystalline phase have a profound effect on the kinetics of nucleation, and oxygen can have an effect on these energies. The oxygen which diffuses into the samples may also have an effect on the stability of phases present and upon the rate of grain growth. Suzuki and co-workers [1, 2] found that the alloy studied here exhibited virtually no grain growth in the

centre of the ribbons when it was heat-treated in the range 723–950 K. They concluded [2] that within this temperature range a residual amorphous phase limits the grain growth, as is the case in the structurally similar alloy of composition $Fe_{73.5}Nb_3Cu_1Si_{13.5}B_9$ studied by Yoshizawa, Oguma and Yamauchi [10]. These observations are pertinent to the current research because all b.c.c. surface grains observed here underwent dramatic growth at temperatures lower than those at which Suzuki and co-workers found no grain growth. The alloy studied here may differ slightly in composition than that studied by Suzuki and co-workers, but it is not clear why such a dramatic difference in growth behaviour would be seen. One possibility is that oxygen diffusion into the surface and/or diffusion of Zr and B to the oxide layer on the outer surface could have destabilized the residual amorphous film between the surface grains, thus permitting grain growth.

Given the high driving force available for growth of the small grains observed here, the pronounced grain coarsening observed in heat-treated samples would not be surprising but for the observation of Suzuki and co-workers [1, 2] that grain sizes are stable over a wide temperature range in this alloy. That the crystals should have remained single phase b.c.c. is surprising, however, since the equilibrium solubilities for both Zr and B in Fe are well below those present in the alloy studied. Suzuki *et al.* [2] reported that the b.c.c. phase formed in this alloy initially maintained all of the Zr and B in solid solution, an unusual situation since grain boundaries might be expected to help catalyse nucleation of the other crystalline phases. The presence of an amorphous film at the grain boundaries would render them ineffective for this catalysis, but the pronounced grain growth going on at the surfaces observed here makes it clear that no such film is present. Because there are no amorphous films present, it appears that the b.c.c. grain boundaries are not effective in catalysing nucleation of the equilibrium phases.

Perhaps the most unusual observation of the present study is the bulging of the glass surface adjacent to the small crystallites shown in Figs 5 and 6. We know of no previous study reporting curvature effects in the glass surrounding surface nucleated crystals. The elevated ridge surrounding the crystals almost surely formed at temperatures above the glass transition temperature, for, if they were caused by strain effects associated with growth of crystallites within the glass, the distortions would not exhibit the continuous curvatures observed here. There has been no measure of the glass transition temperature in this alloy, but it is certainly above the heat treating temperature range employed. Assuming that the crystallites evident in Fig. 5 did form in the molten alloy, with the uncrystallized portion of the ribbon subsequently transforming to a glass during further cooling, then a reasonable explanation on the mounded perimeter is possible. This explanation is based upon the recognition that curvature would result from the balancing of forces on the interfaces which bound the perimeter of the crystallites. This force balance is given by the force balance

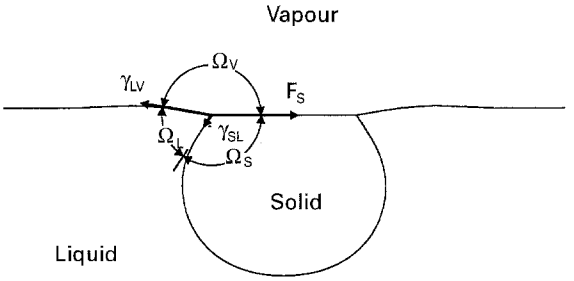

Figure 16 Schematic illustration of surface nucleated crystal of nearly spherical shape. The magnitude and directions of the arrows represent the force balance at solid/liquid/vapour junction.

equation

$$\frac{\gamma_{LV}}{\sin\Omega_S} = \frac{\gamma_{SL}}{\sin\Omega_V} = \frac{F_S}{\sin\Omega_L} \quad (1)$$

in which F_S is the solid/vapour interfacial free energy (frequently termed the surface energy), γ_{LV} is the liquid/vapour interfacial free energy (frequently termed the surface tension), γ_{SL} is the liquid/solid interfacial free energy, and the dihedral angles Ω are those represented in Fig. 16, which shows a crystal (which is here assumed to be nearly spherical) floating at the surface of a melt, with both crystal and melt in contact with the vapour phase. It is unfortunately true that the force balance represented by this equation contains six unknowns, none of which can be specified with any certainty. Useful conclusions can, however be drawn by putting reasonable limits on some of these. One immediate conclusion is that if F_S is equal to or greater than the sum of γ_{LV} and γ_{SL}, then crystals will never nucleate on the free surface, for the liquid will wet the crystal and it can then only nucleate homogeneously or at some heterogeneity. Unfortunately, data for all three interfacial free energies is only available for a few pure metals, and uncertainties in this data is so great (see, for example, Keene [11]) that no confidence can be placed in differences taken. It is therefore impossible to conclude from the published data how frequently crystallites will nucleate at the free surface as observed here.

Despite the lack of accurate data, one can see from Fig. 16 and the force balance equation that if F_S is less than the sum of γ_{LV} and γ_{SL}, and if crystallites do nucleate at the free surface, then the liquid surface must slope upward from the (horizontal) crystallite surface. As an illustration of the range of inclination which might be expected with reasonable surface energies, the set of equalities represented by the force balance equation were solved as a function of γ_{SL}/γ_{LV}, assuming that $\gamma_{LV} = 0.9F_S$. Part of the results of these calculations are shown in Fig. 17, wherein the angle of inclination equals $180° - \Omega_V$. One can see from this figure that liquid surface tilts of a few degrees can occur with reasonable surface energy ratios. Another conclusion which can be drawn from the force balance equation is that if F_S is greater than γ_{LV}, as one would expect, then the crystalline precipitate must extend beyond the melt/solid interface evident on the free surface. How far it will extend under the liquid depends

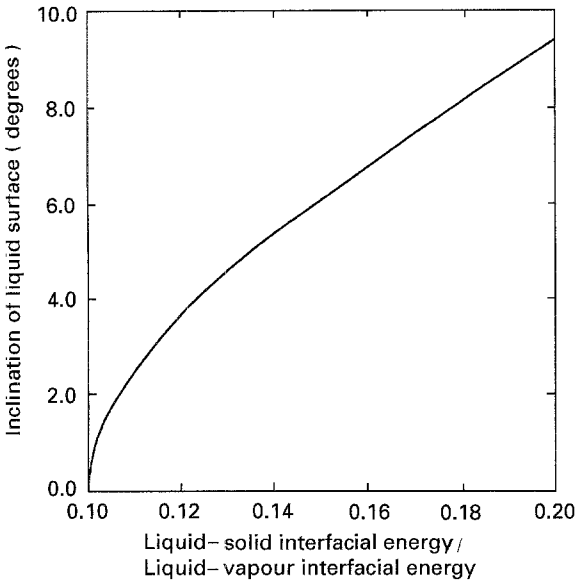

Figure 17 Angle of inclination of the liquid/vapour interface at the three-phase junction of Fig. 16, calculated under the assumption that the liquid/vapour interfacial free energy is 0.9 times as large as the solid/vapour interfacial free energy.

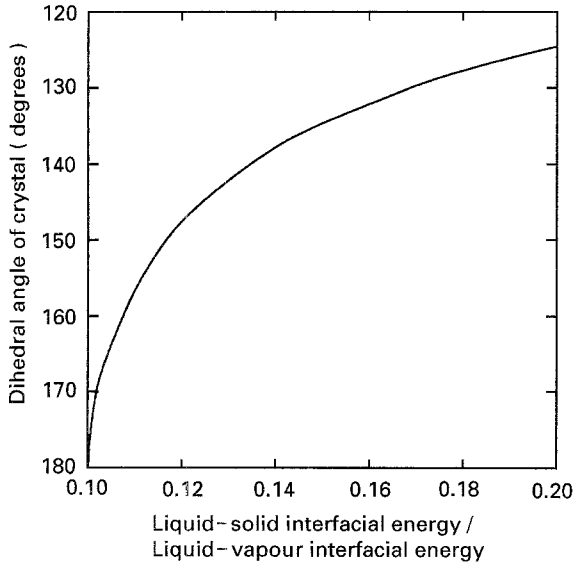

Figure 18 Angle between the solid/vapour interface and the solid/liquid interface, calculated with the same assumption as in Fig. 17.

on the surface energy balance and upon the shapes of the thermal or solute diffusion fields surrounding the crystallite. The angle between the solid/liquid interface and the solid/vapour (Ω_S) was calculated simultaneously with surface tilting shown in Fig. 17, and the results are shown in Fig. 18. This figure shows that Ω_S varies more rapidly with the surface energy ratios than does Ω_V, so very accurate surface energy values would be needed to predict the initial inclination of the solid/liquid interface.

The schematic of a precipitate shown in Fig. 16 is drawn with a planar solid/vapour interface, but the surface profile shown in Fig. 6 makes it clear that the exposed surface of the crystallite is concave. The concave surface could develop quite naturally, however, from a nucleus of the shape shown in Fig. 16. This would follow as a natural consequence of the fact that the solid/liquid interface would move into the liquid at the free surface by migrating up the inclined surface. Maintenance of equilibrium would force the liquid surface to adopt an even greater inclination to compensate for the slight inclination of the newly forming crystalline material, creating an even greater reason for the next increment of new crystal to be inclined upward. This increasing inclination of the liquid free surface would not continue indefinitely, but might easily cause a measurable increase in the apparent tilt at the solid/melt interface. It could also cause a continuously varying curvature of the precipitate surface, as is observed. Motion of the solid/liquid interface up the curved surface would begin very early in the growth process, so one should not expect to see the flat initial surface drawn in Fig. 16.

While the arguments just presented provide a rationale for the appearance of the crystallites evident in Fig. 5, they do not explain the relationship of these structures to similar ones without the surrounding ridge seen in other portions of as-melt-spun ribbons or those seen in heat treated samples (see Fig. 9), which are not surrounded by an elevated ridge. While these crystallites are similar in some respects to those with ridges, they are more angular in appearance. There is no obvious reason why the two types of similar crystallites should have been produced. It may be that the crystallites without ridges formed at lower temperatures where the parent liquid (or glass) was too viscous to bulge under the action of the surface forces, or it may be that different surface chemistries are somehow responsible for the different morphologies.

Even though there is no way to be certain if the small crystallites evident in Fig. 9(a) formed during the initial quench or during the subsequent heat treatment, the protruding nature of the crystallites in Fig. 10 suggest that surface crystallites nucleated during the heat treatments are fundamentally different in nature than those formed during the initial quench. Because the X-ray results demonstrate that randomly oriented crystallites account for more of the growth during heat treatment then do the (200) oriented crystals present after the initial quench, it seems reasonable to conclude that the new surface crystals are randomly oriented. This implies that surface energy effects are less important during the nucleation of crystals at the surface of the glass than they are when the parent phase is a liquid.

Fig. 16 shows the surface dropping down from a maximum height to a lower level away from the precipitate, in accord with experimental observations on those crystallites surrounded by ridges. Nothing so far mentioned explains why this maximum should exist. The crystals are expected to be slightly more dense than the melt, so, even if surface energy effects were not important, the crystals might lie at a lower level than the distant liquid surface, but this does not explain why the maximum exists. It seems likely that a full explanation of the maximum would demonstrate that it must be present to prevent unreasonably high gradients in the surface curvature.

Some of the surface morphologies observed on both as-melt-spun and heat-treated samples are different in appearence from any previously reported. The crystallites evident in Figs 5 and 9 bear some similarity to the holes reported by Watanabe and Nakamura [8], but we find no central bumps, while the bumps in their alloy apparently represented the full extent of the crystallites, with the holes having been formed as material diffused to the crystallites. Again, the bumps evident in Fig. 10 bear a superficial resemblance to the protrusions reported by Watanabe and Nakamura, but those seen here have substantially lower height to breadth ratios. Earlier studies (see, for example, Slawska-Waniewska *et al.* [12] and Scandella *et al.* [13]) found crystallites of differing morphology but show insufficient detail to permit reasonable comparisons. There seems to be good reason to believe that crystallites of many different morphologies can form in alloys of different composition and with different surface contaminants. The range of possibilities is further extended by the possibility of forming crystallites either during the initial quench (above or below the glass transition temperature) or during subsequent heat treatments over a wide range of temperatures.

5. Conclusions

An alloy of nominal composition $Fe_{87}Zr_7B_5Cu_1$ produced in the form of melt-quenched ribbon had many areas covered with crystallites a few tens of nanometres across. X-ray diffractometry showed these crystallites to have the b.c.c. structure and to exhibit a strong (2 0 0) texture. Heat treatment of the ribbons in the temperature range 623–773 K caused additional crystallization to occur, but at all temperatures the (1 1 0) diffraction peak grew more rapidly than that for (2 0 0), indication that randomly oriented crystals were nucleated.

Many of the surface-nucleated crystallites exhibit curvature at the crystal/glass interface which suggests that nucleation at the free surface was made easier by surface energy effects which lowered the nucleation barrier. All crystallites present after melt spinning were recessed into the ribbon surface, but crystallites formed during the heat treatments protrude above the glass surface.

Surface crystals grew rapidly during heat treatments at the higher temperatures employed, and the surface grains developed pronounced faceting which could only be observed by AFM. The rapid grain growth suggests that no glassy phase remained at the surface, though X-ray diffraction studies demonstrated that the samples remained partially amorphous.

Variations in crystallite morphology in as-melt-spun and in heat-treated surfaces suggested that chemical inhomogeneities were present. This was substantiated by energy dispersive spectroscopy, which showed that regions with low Zr concentrations had larger crystallites in heat-treated samples.

Scanning Auger microprobe analysis showed that as-melt-spun surfaces are contaminated with oxygen to a depth of about 8 nm. During heat treatments the oxygen-enriched surface does not become dramatically thicker, but oxygen concentration increases to a few percent at depths greater than 25 nm. This oxygen may affect the morphology and growth kinetics of the surface crystallites.

References

1. K. SUZUKI, A. MAKINO, N. KATAOKA, A. INOUE and T. MASUMOTO, *Mat Trans., JIM* **32** (1991) 93.
2. K. SUZUKI, M. KIKUCHI, A. MAKINO, A. INOUE and T. MASUMOTO, *Ibid.* **32** (1991) 961.
3. U. KÖSTER, *Mater. Sci. Engnr* **97** (1988) 233.
4. M. MATSUURA, *J. Phys. F: Met. Phys.* **15** (1985) 257.
5. K. NAGATA, T. HOSOMA and H. INO, in Proceedings of the 4th International Conference on Rapidly Quenched Metals, (Japan Institute of Metals, Sendai, 1981) p. 635.
6. A. SCHERER and O.T. INAL, *J. Mater. Sci.* **22** (1987) 193.
7. M. FUJINAMI and Y. UJIHIRA, *J. Appl. Phys.* **59** 2387 (1986).
8. Y. WATANABE and Y. NAKAMURA, *J. Mater. Res.* **7** (1992) 2126.
9. L.E. DAVIS, N.C. MACDONALD, P.W. PALMBERG, G.E. RIACH, and R.E. WEBER, "Handbook of auger spectroscopy," second edition, (Perkin-Elmer Corp., Eden Prairie, MN, 1978) pp. 13–15.
10. Y. YOSHIZAWA, S. OGUMA and K. YAMAUCHI, *J. Appl. Phys.* **64** (1988) 6044.
11. B.J. KEENE, "International Materials Reviews," 33, No. 1 (1988) 1.
12. A. SLAWSKA-WANIEWSKA, A. WITEK, and A. REICH, *Mater. Sci. Engnr.* **A133** (1991) 363.
13. L. SCANDELLA, U. STAUFER, D. BRODBECK, P. REIMANN, H.-J. GÜNTHERRODT, R. ZEHRINGER, R. HAUERT, and E.M. MOSER. *Ibid.* **A133** (1991) 601.

Received 8 September 1994
and accepted 23 February 1995